Title

Identification of molecular determinants governing KIF4 cargo recognition of NTCP and their role in HBV/HDV infection

Authors

Sameh A. Gad[1,2*], Doaa A. Abo Elwafa[1,3,4], Masaaki Toyama[1], Mitsunori Ikeguchi[5], Ikuo Shoji[6], Kazuaki Chayama[7,8], Masanori Isogawa[1], Takaji Wakita[1], Hussein H. Aly[1#]

Affiliation

[1]Department of Virology II, National Institute of Infectious Diseases; Japan Institute for Health Security; 1-23-1 Toyama; Shinjuku-ku: Tokyo 162-8640; Japan

[2]Department of Microbiology and Immunology; Faculty of Pharmacy; Minia University; Minia 61519; Egypt

[3]Graduate School of Medical and Pharmaceutical Sciences, Chiba University, Japan

[4]Department of Medical Microbiology and Immunology, Faculty of Medicine, South Valley University, Egypt

[5]Computational Life Science Laboratory, Graduate School of Medical Life Science, Yokohama City University, Yokohama, Japan

[6]Division of Infectious Disease Control; Center for Infectious Diseases; Kobe University Graduate School of Medicine; 7-5-1 Kusunoki-cho; Chuo-ku Kobe 650-0017; Japan

[7]Hiroshima Institute of Life Sciences; Hiroshima; Japan

[8]RIKEN Center for Integrative Medical Sciences; Yokohama; Japan

Running title

KIF4 Recognition of NTCP regulating HBV/HDV entry.

[#] **Address correspondence to:** Hussein H. Aly, hussein.a@jihs.go.jp

[*] **Present address:** Department of Virology, Graduate School of Medical and Dental Sciences, Niigata University, Niigata, Japan. (Recent affiliation)

Abstract word count: 232, Text word count: 4514

Abstract

The surface availability of the sodium taurocholate co-transporting polypeptide (NTCP), which serves as entry receptor for Hepatitis B virus (HBV) and Hepatitis D virus (HDV), is a key determinant of HBV/HDV infectivity. We previously identified the Kinesin motor protein KIF4 as a key regulator of NTCP trafficking to the plasma membrane. However, the molecular mechanism by which NTCP is recognized as a KIF4 transport cargo has remained undefined. Here, we identified a leucine-rich motif, LLLI (aa 298–301), within the C-terminal transmembrane domain of NTCP as an essential determinant for KIF4 transport. Co-immunoprecipitation analyses revealed its importance for NTCP interaction with KIF4. This motif is conserved in another established KIF4 cargo, integrin β1 (ITGB1), and mutation of the corresponding residues similarly disrupted ITGB1–KIF4 interaction, indicating a shared cargo recognition mechanism employed by KIF4. Functionally, disruption of the NTCP leucine-rich motif markedly impaired NTCP surface localization without affecting total protein expression, resulting in severe attenuation of HBV and HDV infection. Structural modeling and computational protein–protein interaction analysis indicated that the mutation does not alter NTCP structure or NTCP/preS1 binding affinity, supporting a trafficking-specific defect. Substitution mutations identified L298 and L299 as the minimal residues required for interaction with KIF4. Our findings define a recognition motif that regulates KIF4-dependent cargo identification and surface trafficking. It also underscores the potential of targeting KIF4-mediated NTCP recognition and transport to inhibit HBV and HDV entry.

Importance

Hepatitis B and D viruses require the hepatocyte surface receptor NTCP for entry. We identified a conserved leucine-rich motif (LLLI, aa 298–301) in NTCP that is necessary for its recognition by the kinesin motor KIF4; disrupting this motif selectively impairs NTCP surface trafficking and markedly attenuates HBV/HDV infection without reducing total NTCP or intrinsic receptor function. Importantly, we identified a similar motif in integrin β1 (ITGB1; aa 747–750) that is required for interaction with KIF4, revealing a similar cargo selection mechanism for different proteins. Scientifically, these findings define a motif-derived cargo-selection determinant implied by KIF4, advancing a general principle for kinesin-dependent cargo recognition. More broadly, this work highlights a possible host-directed antiviral approach that targets cargo-selection interfaces and provides a conceptual framework for manipulating kinesin-mediated trafficking of clinically relevant membrane proteins beyond NTCP, with implications for receptor regulation and membrane protein therapeutics.

Introduction

Chronic hepatitis B virus (HBV) infection remains a major global health burden, affecting nearly 1.5 million new infections/year with 254 million individuals suffering from chronic HBV worldwide. Chronic HBV patients may progress to complications from the progressive liver disease such as cirrhosis, and hepatocellular carcinoma (1). Clinical outcomes of HBV patients worsen substantially in the presence of hepatitis D virus (HDV), a defective satellite virus that requires HBV envelope proteins for propagation. HDV coinfection accelerates liver inflammation, increases the risk of fulminant hepatitis, and markedly elevates the likelihood of end-stage liver disease (2). A pivotal step in the life cycle of both HBV and HDV is their shared dependence on the sodium taurocholate co-transporting polypeptide (NTCP), a bile acid transporter that functions as the essential entry receptor on hepatocytes (3). Understanding how NTCP is trafficked and presented on the cell surface is therefore central to elucidating the mechanisms governing HBV/HDV infection (4).

Kinesin family member 4 (KIF4) is a microtubule-based motor protein involved in intracellular transport, chromosome segregation, and cytoskeletal organization (5). Beyond its canonical roles in mitosis and nuclear dynamics, emerging evidence indicates that KIF4 also functions in cytoplasmic vesicular trafficking and regulates the transport and surface localization of specific membrane proteins (6-8). Our previous findings revealed that KIF4 interacts with NTCP and facilitates its anterograde transport to the plasma membrane, thereby enabling the receptor's availability for HBV/HDV attachment and viral entry (4). These observations positioned KIF4 as a previously unrecognized host factor that

98 modulates viral susceptibility by controlling NTCP surface expression (4, 9).

99 Although kinesins share highly conserved motor domains, cargo specificity is primarily
100 determined by divergent C-terminal tail domain that engage adaptor proteins, recognize
101 discrete cargo-binding motifs, and integrate regulatory inputs such as post-translational
102 modifications and scaffolding complex assembly (10-13). For many kinesins, such as
103 KIF1A, KIF5, and KIF3 family members, structural studies have identified short linear
104 motifs or coiled-coil regions that mediate selective cargo recognition (11, 12, 14, 15).
105 However, the molecular basis by which KIF4 identifies and transports its physiological
106 cargoes remains poorly defined. Although, we clearly demonstrated the interaction between
107 KIF4 and NTCP by pull-down assays and intracellular localization studies, recombinant
108 KIF4 and NTCP failed to exhibit a direct physical association in vitro. This observation
109 suggests that the KIF4–NTCP interaction is likely facilitated by specific adaptor proteins
110 that mediate or regulate this association within the cellular environment (4). Only limited
111 information exists regarding KIF4's tail-domain interactome, and no detailed determinants
112 have been identified for its cargo selection of membrane proteins such as NTCP. This gap
113 in knowledge reduces our ability to understand how KIF4-dependent cargo trafficking is
114 regulated and how it may be selectively modulated.

115 Defining the molecular determinants that govern KIF4–cargo recognition, particularly in
116 the context of NTCP, holds substantial therapeutic relevance. Because NTCP surface
117 availability is a rate-limiting step for HBV/HDV entry (3, 4), elucidating how KIF4
118 recognizes and transports NTCP could reveal new intervention points for antiviral drug
119 development (4, 9). Targeting the specific interaction interface—rather than globally

120 inhibiting kinesin activity—offers the possibility of selectively disrupting viral entry while
121 preserving essential cellular transport processes. A mechanistic understanding of this cargo
122 recognition pathway may therefore enable the rational design of small molecules or
123 peptides that block NTCP trafficking, providing a novel host-directed strategy to prevent
124 HBV/HDV infection.

125 In this study, we identify the molecular basis by which the kinesin motor protein KIF4
126 recognizes (NTCP and ITGB1) as a transport cargo and regulates its delivery to the
127 hepatocyte plasma membrane. We show that KIF4-mediated transport requires the
128 leucine-rich motif (LLLI) present at the C-terminal transmembrane domain of both
129 membrane proteins. Disruption of this motif abolishes the interaction between KIF4 and its
130 cargo (NTCP or ITGB1), markedly reduces the surface expression of both proteins without
131 affecting total protein levels. As a result, suppression of NTCP surface expression severely
132 impaired HBV and HDV entry. Together, these findings define a previously unrecognized
133 kinesin cargo-recognition motif that controls NTCP surface localization and represents a
134 critical regulatory node in HBV and HDV infection.

135

136 Materials and Methods

137 Cell lines and peptides

138 HepG2 were cultured with DMEM/F-12 + GlutaMax medium (Gibco) supplemented
139 with 10% fetal bovine serum (FBS), 10 mM HEPES, 100 unit/ml penicillin, 100 μg/ml
140 streptomycin, and 5 μg/ml insulin (4). HEK293FT cells were cultured in DMEM, high
141 glucose supplemented with 10% FBS, sodium pyruvate (1 mM), MEM non-essential amino

142 acids (1X), penicillin 100 unit/ml penicillin, 100 μg/ml streptomycin. All cell lines used in
143 this work were incubated at 37 °C in the presence of 5% CO_2 (9). Fluorescent HBV preS1
144 probe, a peptide spanning the 2-48 amino acids of the L-HBsAg preS1 region with
145 myristoylation and 6-carboxytetramethylrhodamine (TAMRA) labeling at N- and C-
146 termini, respectively, was synthesized by Scrum, Inc.

147 **Plasmid Construction**

148 The N-terminal 6×Myc-tagged KIF4 expression construct in the pIRESpuro3 vector was
149 kindly provided by Dr. Toru Hirota (Cancer Institute of the Japanese Foundation for Cancer
150 Research, JFCR) (16). C-terminally HA-tagged full-length NTCP (GenBank Accession No.
151 NM_003049.4), cloned into the CSII-EF-MCS vector at the *XhoI* (5′) and *XbaI* (3′) sites
152 and provided by Dr. Hiroyuki Miyoshi (RIKEN BioResource Research Center, Japan), was
153 subcloned into the pcDNA3.1 expression vector. The NTCP-HA open reading frame (ORF)
154 was excised by *XhoI* and *XbaI* and ligated into *XhoI/XbaI*-digested pcDNA3.1 to generate
155 full-length NTCP-HA in pcDNA3.1.

156 **Generation of full-length NTCP-HA alanine-substitution mutants**

157 The full-length NTCP-HA construct carrying four alanine substitutions (L298A, L299A,
158 L300A, and I301A) was generated by introducing these mutations into wild-type (WT)
159 NTCP-HA using a two-step PCR approach.
160 Two overlapping PCR fragments were first amplified from WT NTCP-HA using the
161 following primer pairs:

162 • **Fragment 1:**

163 Forward 5′-TAACGCTCGAGATGGAGGCCCACAAC-3′

Reverse 5′-CTCATAGCACCAAAATATGGCGGCGGCGGCGGCCCCTTCTCCAAGCTGGAAAATC-3′

- **Fragment 2:**

Forward 5′-GATTTTCCAGCTTGGAGAAGGGGCCGCCGCCGCCGCCATATTTTGGTGCTATGAG-3′

Reverse 5′-GGCCCTCTAGACTAAGCGTAATCTGGAAC-3′

A third PCR reaction was then performed using the two overlapping amplicons as templates, with the forward primer of Fragment 1 and the reverse primer of Fragment 2. The resulting full-length mutated NTCP-HA fragment was digested with *XhoI* and *XbaI* and ligated into *XhoI/XbaI*-digested pcDNA3.1.

Generation of NTCP truncated constructs

Two N-terminal NTCP truncations, NTCP-HA (aa 1–233) and NTCP-HA (aa 1–117), were generated by PCR amplification of WT NTCP-HA using:

- **Forward primer** (both constructs):

5′-TGCCAGGTACCATGGAGGCCCACAAC-3′

- **Reverse primers:**

NTCP-HA (aa 1–233): 5′-TCGGCTCTAGACTAAGCGTAATCTGGAACATCGTATGGGTAGCCAATAAAAGGCATCAGGG-3′

NTCP-HA (aa 1–117): 5′-

186 TCGGCTCTAGACTAAGCGTAATCTGGAACATCGTATGGGTAGTTCATGTCCCC
187 CTTCATGG-3′
188 PCR products were digested with *KpnI* and *XbaI* and subcloned into *KpnI/XbaI*-digested
189 pcDNA3.1.
190 A C-terminal region construct NTCP-HA (aa 234–349) was similarly generated using:
191 • Forward 5′-TGCCAGGTACCATGTTTCTGCTGGGTTATG-3′
192 • Reverse 5′-
193 TCGGCTCTAGACTAAGCGTAATCTGGAACATCGTATGGGTAGGCTGTGCAAGG
194 GGAGCAGT-3′
195 and inserted into *KpnI/XbaI*-digested pcDNA3.1.
196 **Generation of NTCP-HA (aa 234–349) constructs carrying alanine-substitution**
197 **mutations**
198 The truncated NTCP-HA (aa 234–349) construct carrying the quadruple mutation
199 (L298A/L299A/L300A/I301A) was generated using the same overlapping PCR strategy
200 employed for full-length NTCP. Two PCR fragments were amplified from WT NTCP-HA
201 (aa 234–349) using the primer pairs:
202 • **Fragment 1:**
203 Forward 5′-TGCCAGGTACCATGTTTCTGCTGGGTTATG-3′
204 Reverse 5′-
205 CTCATAGCACCAAAATATGGCGGCGGCGGCGGCCCCTTCTCCAAGCTGGAAA
206 ATC-3′
207 • **Fragment 2:**

208 Forward 5′-

209 GATTTTCCAGCTTGGAGAAGGGGCCGCCGCCGCCGCCATATTTTGGTGCTATG

210 AG-3′

211 Reverse 5′-GGCCCTCTAGACTAAGCGTAATCTGGAAC-3′

212 The overlap-extension PCR product was digested with *KpnI* and *XbaI* and subcloned into

213 *KpnI/XbaI*-digested pcDNA3.1.

214 **Generation of NTCP-HA (aa 234–349) single alanine-substitution mutants**

215 Single alanine-substitution mutants of NTCP-HA (aa 234–349) (L298A, L299A, L300A,

216 or I301A) were generated using the same overlap-extension PCR strategy, with WT NTCP-

217 HA (aa 234–349) as the template.

218 For each mutant, two PCR reactions were performed as follows:

219 • **L298A mutant:**

220 PCR reaction 1:

221 Forward: 5′-TGCCAGGTACCATGTTTCTGCTGGGTTATG-3′

222 Reverse: 5′-

223 CTCATAGCACCAAAATATGGCAATGAGGAGGGCCCCTTCTCCAAGCTGGAAA

224 ATC-3′

225 PCR reaction 2:

226 Forward: 5′-

227 GATTTTCCAGCTTGGAGAAGGGGCCCTCCTCATTGCCATATTTTGGTGCTATGA

228 G-3′

229 Reverse: 5′-GGCCCTCTAGACTAAGCGTAATCTGGAAC-3′

230 • **L299A mutant:**

231 PCR reaction 1:

232 Forward: 5′-TGCCAGGTACCATGTTTCTGCTGGGTTATG-3′

233 Reverse: 5′-

234 CTCATAGCACCAAAATATGGCAATGAGGGCAAGCCCTTCTCCAAGCTGGAAA

235 ATC-3′

236 PCR reaction 2:

237 Forward: 5′-

238 GATTTTCCAGCTTGGAGAAGGGCTTGCCCTCATTGCCATATTTTGGTGCTATGA

239 G-3′

240 Reverse: 5′-GGCCCTCTAGACTAAGCGTAATCTGGAAC-3′

241 • **L300A mutant:**

242 PCR reaction 1:

243 Forward: 5′-TGCCAGGTACCATGTTTCTGCTGGGTTATG-3′

244 Reverse: 5′-

245 CTCATAGCACCAAAATATGGCAATGGCGAGAAGCCCTTCTCCAAGCTGGAAA

246 ATC-3′

247 PCR reaction 2:

248 Forward: 5′-

249 GATTTTCCAGCTTGGAGAAGGGCTTCTCGCCATTGCCATATTTTGGTGCTATGA

250 G-3′

251 Reverse: 5′-GGCCCTCTAGACTAAGCGTAATCTGGAAC-3′

252 • **I301A mutant:**

253 PCR reaction 1:

254 Forward: 5′-TGCCAGGTACCATGTTTCTGCTGGGTTATG-3′

255 Reverse: 5′-

256 CTCATAGCACCAAAATATGGCGGCGAGGAGAAGCCCTTCTCCAAGCTGGAAA

257 ATC-3′

258 PCR reaction 2:

259 Forward: 5′-

260 GATTTTCCAGCTTGGAGAAGGGCTTCTCCTCGCCGCCATATTTTGGTGCTATGA

261 G-3′

262 Reverse: 5′-GGCCCTCTAGACTAAGCGTAATCTGGAAC-3′

263 For each mutant, a third PCR reaction was performed using the products of the two

264 reactions as templates, with the forward primer from PCR reaction 1 and the reverse primer

265 from PCR reaction 2. The final PCR products were digested with *KpnI* and *XbaI* and

266 ligated into *KpnI*/*XbaI*-digested pcDNA3.1.

267 **Plasmid transfection**

268 Plasmid transfections in HEK293FT cells were performed using Lipofectamine 2000,

269 whereas transfections in HepG2 cells were carried out using Lipofectamine 3000, in

270 accordance with the manufacturer's instructions.

271 **Immunoblot analysis**

272 Protein expressions were analyzed by immunoblotting as previously described (17). The

273 primary antibodies used were mouse monoclonal anti-Myc (Santa Cruz Biotechnology, sc-

274 40), anti–E-cadherin (Santa Cruz Biotechnology, sc-8426), and anti–β-actin (Sigma-
275 Aldrich, A5441), as well as rabbit polyclonal anti-HA (Sigma-Aldrich, H6908). To assess
276 NTCP expression, protein samples were treated with Peptide-N-Glycosidase F (PNGase F;
277 250 U) prior to SDS–PAGE to remove N-linked glycans from glycosylated NTCP, as
278 previously reported (9).

279 **Isolation of the cell surface proteins**

280 Cell surface proteins were isolated by surface biotinylation followed by streptavidin–
281 agarose affinity purification, as previously described (4). The recovered cell surface
282 fractions were subsequently analyzed by immunoblotting as described above. E-cadherin
283 (CDH1) was used as an internal loading control to verify the enrichment and integrity of
284 the surface protein fraction (18).

285 **Co-immunoprecipitation (Co-IP) assay**

286 HEK293FT cells were co-transfected with the indicated HA-tagged NTCP or HA-tagged
287 ITGB1 expression plasmids together with a Myc-tagged KIF4 expression plasmid at a 1:1
288 DNA ratio. At 72 h post-transfection, cells were harvested and lysed, and protein complexes
289 were subjected to co-immunoprecipitation (co-IP) using a mouse monoclonal anti-Myc
290 antibody (Santa Cruz Biotechnology, sc-40). Mouse normal IgG was used in parallel as a
291 negative control to assess assay specificity. Following immunoprecipitation, the recovered
292 complexes were analyzed by immunoblotting to detect co-immunoprecipitated HA-tagged
293 NTCP or HA-tagged ITGB1 in the pull-down fraction. Cell lysis and co-IP procedures were
294 performed using the Pierce Co-Immunoprecipitation Kit (Thermo Fisher Scientific, 26149)
295 in accordance with the manufacturer's instructions.

296 **HBV preS1 peptide binding assay**

297 Cell surface attachment of the N-terminally myristoylated and C-terminally TAMRA-
298 labeled HBV preS1 peptide was assessed in HepG2 cells transiently expressing hNTCP as
299 previously described (9).

300 **HBV infection assay**

301 HBV viral inoculum was prepared from the culture supernatant of HepAD38.7-Tet cells
302 as previously described (19). HepG2 cells transiently expressing hNTCP were inoculated
303 with HBV at a multiplicity corresponding to 10,000 genome equivalents (GEq) per cell in
304 the presence of 4% PEG8000. Following a 16-h incubation, unbound viral particles were
305 removed by extensive washing, and cells were maintained in culture for an additional 7
306 days. HBV infection was assessed by quantifying secreted HBeAg using ELISA and
307 intracellular HBV pgRNA levels by real-time RT-PCR.

308 **HDV infection assay**

309 HDV used in infection experiments was generated from the culture supernatant of Huh7
310 cells co-transfected with pSVLD3 and pT7HB2.7 plasmids, as previously described (20,
311 21). HepG2 cells transiently expressing hNTCP were inoculated with HDV at 100 GEq per
312 cell in the presence of 5% PEG8000. After a 16-h incubation, unbound virus was removed
313 by extensive washing, and the cells were maintained in culture for an additional 6 days.
314 HDV infection was evaluated by detection of HDAg using immunofluorescence analysis.

315 **Immunofluorescence (IF) assay**

316 Immunofluorescence staining was performed as previously described (4). Briefly, cells
317 were fixed with 4% paraformaldehyde and permeabilized with 0.3% Triton X-100. The

318 samples were then incubated with a rabbit anti-HDAg primary antibody (developed by
319 Scrum), followed by incubation with an Alexa Fluor 555–conjugated secondary antibody.
320 Nuclei were counterstained with DAPI. Fluorescence signals were examined and imaged
321 using a fluorescence microscope.

322 **Structural prediction and comparative analysis of NTCP**

323 The three-dimensional structures of wild-type NTCP and the NTCP mutants were
324 predicted using AlphaFold 3.0.0 installed on a local server. The default databases were
325 used, including the Google DeepMind–curated versions of BFD, MGnify (v2022_05),
326 UniProt (2021_04), UniRef90 (2022_05), PDB, and PDB_seqres (2022_09_08). The wild-
327 type NTCP sequence was obtained from UniProt (Q14973). For the mutants L298A,
328 L299A, L300A, I301A, and the quadruple mutant L298A/L299A/L300A/I301A, the
329 corresponding residues in the sequence were modified accordingly. For each prediction, a
330 single random seed was used, and among the five generated output models, the structure
331 with the highest confidence score was selected. RMSD calculations were performed using
332 the Cα atoms of residues 22–309.

333 **Amino acid sequence alignment**

334 Multiple sequence alignments were performed for the C-terminal 116 amino acids of NTCP
335 (aa 234–349) in comparison with human ITGB1, as well as for the NTCP C-terminal
336 transmembrane sequence (aa 294–305) across HBV-susceptible species. Alignments were
337 generated using the Clustal Omega algorithm (EMBL-EBI web server) with default
338 parameters. Graphical representations of sequence conservation and alignment annotations
339 were prepared using ESPript 3.2 (22-24).

340 **Statistical analysis**

341 All experiments were performed in triplicate, and data represent the mean ± standard
342 deviation (SD) from three independent experiments. Statistical significance was assessed
343 using an unpaired two-tailed Student's *t* test (**, $P < 0.01$; ***, $P < 0.001$; NS, not
344 significant).

345

346 ## Results:

347 **The C-terminal Domain of NTCP is crucial for interaction with KIF4**

348 We previously demonstrated that KIF4 mediates NTCP trafficking to the hepatocyte cell
349 surface(4). To further clarify the mechanism by which KIF4 recognizes and interacts with
350 its cargo, we constructed expression plasmids encoding C-terminal HA-tagged full-length
351 NTCP, as well as NTCP truncation mutants containing either the first 117 or 233 amino
352 acids (Fig. 1A). Each NTCP construct was separately co-transfected with a Myc-tagged
353 KIF4 expression plasmid into HEK293FT cells and incubated for 72 hours, after which co-
354 immunoprecipitation (co-IP) assays were performed. Immunoprecipitation with the anti-
355 Myc antibody resulted in efficient recovery of KIF4, while no KIF4 was detected in
356 samples processed with the isotype control antibody, thereby validating the specificity of
357 the assay (Fig. 1B). Notably, co-immunoprecipitation analysis demonstrated that KIF4
358 selectively associates with the full-length NTCP, whereas truncated NTCP variants failed to
359 associate with KIF4 (Fig. 1B), indicating that the interaction between NTCP and KIF4
360 requires the C-terminal region of NTCP.

361 **A leucine-rich motif (aa 298–301) in the C-terminal region of NTCP is essential for its**

362 **interaction with KIF4.**

363 In addition to NTCP, KIF4 has been reported to mediate the intracellular transport of
364 other host proteins, including human integrin β1 (ITGB1) (25). This raises the possibility
365 that shared functional determinants within these cargo proteins mediate their recognition by
366 KIF4. To identify candidate motifs within the NTCP C-terminal region that may be
367 responsible for KIF4 interaction, we aligned the amino acid sequence of the NTCP C-
368 terminal 116 residues (aa 234–349) with human ITGB1 sequence (Fig. 2A) (Fig. S1). The
369 alignment revealed that the NTCP C-terminal transmembrane domain (C-TMD; aa 281–
370 311) contains a leucine-rich motif (LLLI; aa 298–301), which is also present within the C-
371 TMD of ITGB1 (aa 729–751) at positions 747–750. This conservation suggested that the
372 LLLI motif might function as a determinant for KIF4 recognition. To experimentally
373 evaluate this hypothesis, we generated expression constructs encoding C-terminal HA-
374 tagged NTCP fragments comprising aa 234–349, either wild-type or carrying an alanine-
375 substitution mutation (AAAA) in place of the LLLI motif (Fig. 2B). Each construct was
376 individually co-transfected with a Myc-tagged KIF4 expression plasmid into HEK293FT
377 cells for 72 h, followed by co-IP analysis. Immunoprecipitation with anti-Myc antibody
378 efficiently recovered KIF4, whereas the isotype control yielded no detectable signal,
379 validating the specificity of the assay (Fig. 2C). Both full-length NTCP and the wild-type
380 NTCP (aa 234-349) fragment co-immunoprecipitated with KIF4. In contrast, the AAAA
381 mutant failed to associate with KIF4 (Fig. 2C). These results suggest that the leucine-rich
382 LLLI motif (aa 298–301) within the NTCP C-terminal region is essential for its interaction
383 with KIF4 and likely constitutes a key determinant for KIF4-dependent cargo recognition.

384 **A conserved leucine-rich motif within the C-terminal region of ITGB1 (aa 747–750) is**
385 **critical for KIF4-mediated recognition**

386 To further assess the functional importance of the leucine-rich motif (LLLI; aa 747–750)
387 located within the C-TMD of ITGB1 in mediating ITGB1–KIF4 interaction, we
388 constructed expression plasmids encoding C-terminal HA-tagged full-length ITGB1 in
389 either WT form or containing alanine mutations (AAAA) substituting the LLLI motif (Fig.
390 3A). Each construct was individually co-transfected with a Myc-tagged KIF4 expression
391 vector into HEK293FT cells for 72 h, followed by co-IP analysis. Immunoprecipitation
392 with an anti-Myc antibody efficiently recovered KIF4, whereas no signal was obtained with
393 the isotype control antibody, confirming assay validity (Fig. 3B). Remarkably, WT full-
394 length ITGB1 co-immunoprecipitated with KIF4, whereas the AAAA mutant did not (Fig.
395 3B). These results indicate that the leucine-rich LLLI motif (aa 747–750) within the ITGB1
396 C-TMD is crucial for KIF4-dependent recognition and interaction with ITGB1.

397 **The C-terminal leucine-rich motif (aa 298–301) of NTCP is crucial for KIF4-mediated**
398 **NTCP surface transport and efficient NTCP-dependent HBV/HDV infection**

399 Given that NTCP is transported to the hepatocyte cell surface along microtubules by KIF4
400 to facilitate HBV and HDV entry (4), we investigated the functional importance of the C-
401 terminal leucine-rich motif of NTCP (aa 298–301) in KIF4-mediated surface NTCP
402 trafficking and HBV/HDV infection. To this end, we created expression plasmids encoding
403 C-terminally HA-tagged full-length NTCP, either as the wild-type ($NTCP^{WT}$) or with
404 alanine substitutions in the LLLI motif ($NTCP^{AAAA}$). HepG2 cells transiently expressing
405 $NTCP^{WT}$ or $NTCP^{AAAA}$ for 72 h were exposed to biotinylation-based surface labeling assay

406 to selectively tag and purify cell surface protein fractions. Although total NTCP expression
407 levels were comparable between the two constructs (Fig. 4A, input), $NTCP^{AAAA}$ exhibited
408 markedly reduced surface localization relative to $NTCP^{WT}$, which predominantly localized
409 to the cell membrane (Fig. 4A, surface). Consistent with impaired surface expression,
410 $NTCP^{AAAA}$ expressing cells displayed significantly reduced binding of the HBV preS1
411 peptide ($P < 0.001$) (Fig. 4B and C). Furthermore, HBV infection was strongly attenuated
412 in $NTCP^{AAAA}$ expressing cells, as evidenced by a significant reduction in intracellular HBV
413 pgRNA levels ($P < 0.001$) (Fig. 4D and E) and HBeAg secreted in the cell culture
414 supernatant ($P < 0.001$) (Fig. 4F) compared with $NTCP^{WT}$ expressing cells. Similarly, HDV
415 infection was substantially decreased in $NTCP^{AAAA}$ expressing cells, as demonstrated by a
416 marked reduction in HDAg positive cells ($P < 0.001$) (Fig. 4G and H). Importantly, the
417 $NTCP^{AAAA}$ substitution did not adversely affect cell viability relative to $NTCP^{WT}$ (Fig. 4I),
418 excluding cytotoxic effects. Collectively, these results demonstrate that the NTCP C-
419 terminal leucine-rich motif (aa 298–301) is essential for KIF4-mediated NTCP surface
420 transport and is consequently critical for efficient HBV and HDV entry.

421 **Structural modeling demonstrates that the $NTCP^{AAAA}$ substitution mutation does not**
422 **directly alter NTCP's binding affinity for the preS1 domain**

423 Additionally, we conducted an *in silico* structural analysis using AlphaFold3 (26) to
424 predict the three-dimensional structures of $NTCP^{WT}$, the single alanine-substitution mutants
425 $NTCP^{L298A}$, $NTCP^{L299A}$, $NTCP^{L300A}$, and $NTCP^{I301A}$, and the quadruple mutant $NTCP^{AAAA}$.
426 The overall predicted folds were nearly identical across all variants, with root mean squared
427 deviations (RMSDs) of ≤ 0.3 Å relative to $NTCP^{WT}$ (Fig. 5A, a-f). A close-up view of the

428 mutated C-terminal region likewise revealed no discernible local structural perturbations
429 (Fig. 5A, g). Because cell surface expressed NTCP mediates HBV entry through binding to
430 the preS1 domain of the large hepatitis B surface protein (LHBs) on hepatocytes (3), we
431 next assessed whether the AAAA substitution directly affects NTCP–preS1 interaction. To
432 this end, we employed DDMut-PPI (27), a deep learning–based model that predicts changes
433 in protein–protein interaction binding free energy upon multiple amino acid substitutions
434 (28). The predicted affinity change ($\Delta\Delta G^{\text{Affinity WT}\rightarrow\text{L298A, L299A, L300A, I301A}}$) was -1.11
435 kcal/mol (root mean squared error: 1.33 kcal/mol), predicting no substantial reduction in
436 the intrinsic binding affinity between NTCP and the HBV preS1 domain (Fig. 5B and C).
437 Collectively, these *in silico* analyses support the conclusion that the impaired ability of the
438 $NTCP^{AAAA}$ mutant to support HBV and HDV infection results from defective surface
439 trafficking rather than from a direct disruption of NTCP–preS1 binding.

440 **L298 and L299 of NTCP constitute the minimal critical residues required for**
441 **mediating the interaction between NTCP and KIF4**

442 As our results indicated that the NTCP leucine-rich motif (aa 298–301) is required for its
443 interaction with KIF4 and subsequent surface transport, we next sought to define the
444 minimal residues within this motif that mediate the interaction. To this end, we generated
445 expression plasmids encoding C-terminal HA-tagged NTCP fragments spanning aa 234–
446 349, either wild-type or carrying a single alanine substitution at L298, L299, L300, or I301
447 (Fig. 6A). Each construct was co-transfected with a Myc-tagged KIF4 expression plasmid
448 into HEK293FT cells for 72 h, followed by co-IP analysis. Immunoprecipitation with an
449 anti-Myc antibody efficiently recovered KIF4, whereas the isotype control yielded no

450 detectable signal, validating the assay specificity (Fig. 6B). The wild-type NTCP fragment
451 (aa 234–349), as well as the L300A and I301A variants, robustly co-immunoprecipitated
452 with KIF4. In contrast, fragments carrying L298A or L299A exhibited absent or markedly
453 reduced co-IP signals. As expected, the AAAA mutant fragment used as a negative control
454 failed to associate with KIF4 (Fig. 6B), further validating the co-IP specificity. Taken
455 together, these findings indicate that NTCP residues L298 and L299 represent the minimal
456 and essential determinants required for efficient NTCP–KIF4 interaction.
457

458 ## Discussion

459 ATP-dependent intracellular transport of cargo proteins along microtubule networks by
460 motor proteins is a fundamental process required for cellular homeostasis. Microtubule-
461 based motors, primarily kinesins and dyneins, are ATP-driven transporters that mediate the
462 directional trafficking of diverse intracellular cargos. Kinesins generally drive anterograde
463 transport toward the cell periphery, whereas dyneins and certain C-terminal kinesins
464 facilitate retrograde movement toward the perinuclear region (10). A growing body of
465 evidence demonstrates that these motor proteins play critical roles in viral infection by
466 directly interacting with viral components, thereby promoting viral replication and
467 propagation (29-32). In addition, we and others have shown that viruses can indirectly
468 exploit the kinesin transport machinery by engaging host proteins that are transported by
469 motor proteins and subsequently co-opted to support viral entry or replication (4, 25, 33).
470 Notably, the motor protein KIF4 interacts with and anterogradely transports several host
471 proteins, including human sodium taurocholate co-transporting polypeptide (NTCP), to the

472 hepatocyte cell surface, where NTCP serves as an entry receptor for HBV and HDV. KIF4
473 has also been reported to transport integrin β1 (ITGB1) and L1 cell adhesion molecule
474 (L1CAM)–containing vesicles in developing cortical neurons (4, 7, 25). These observations
475 raise the question of how KIF4 selectively recognizes and transports specific host cargos.
476 Structurally, KIF4 contains an N-terminal ATPase motor domain responsible for
477 microtubule engagement and a C-terminal cargo-binding tail that mediates cargo
478 recognition (10). In the present study, we used NTCP and ITGB1 as model cargos to
479 interrogate the molecular basis of KIF4-mediated transport.

480 Through a combination of amino acid sequence alignment and biochemical analyses, we
481 identified a conserved C-terminal leucine-rich motif in both NTCP (aa 298–301) and
482 ITGB1 (aa 747–750) that is essential for cargo recognition and transport mediated by KIF4.
483 NTCP is a liver-specific, basolaterally expressed transporter that mediates the hepatic
484 uptake of bile acids and functions as the bona fide entry receptor for HBV and HDV viruses
485 (3, 34). In this study, alanine substitution of the NTCP leucine-rich motif (aa 298–301)
486 disrupted normal NTCP surface localization, markedly reduced binding of a fluorescent
487 HBV preS1 probe, and significantly attenuated HBV and HDV infection (Fig. 4). These
488 findings underscore the functional importance of this motif in KIF4-mediated NTCP
489 trafficking to the cell surface.

490 Although several NTCP orthologs from different species support HBV binding and
491 infection (35, 36), sequence alignment of the C-terminal transmembrane sequence (aa 294–
492 305) revealed that the putative leucine-rich motif (aa 298–301) is not strictly conserved
493 among HBV-susceptible species (Fig. S3). The fact that this motif is not fully conserved

494 among different species supporting HBV infection suggests it does not play a direct role in
495 mediating NTCP binding to the HBV preS1 domain. Instead, it may possess a function
496 unique to the host cell, most likely in regulating the intracellular trafficking of NTCP, rather
497 than directly facilitating viral binding to NTCP. Consistent with this interpretation, *in*
498 *silico* structural modeling using AlphaFold supported that alanine substitution of this motif
499 does not induce detectable global or local conformational changes in NTCP (Fig. 5).
500 Comparison with the experimentally determined human NTCP cryo-EM structure (PDB:
501 7PQG) showed that all AlphaFold3 models most closely resembled the inward-facing
502 conformation, with an RMSD of approximately 1.5 Å (34), and no mutation-associated
503 structural perturbations were predicted. This apparent structural insensitivity may reflect
504 inherent limitations of machine-learning–based prediction, which tends to favor
505 conformations represented in the training data, or alternatively suggests that NTCP may
506 adopt distinct, context-dependent conformational states influenced by membrane
507 environment or interacting partners that are not captured by isolated *in silico* modeling. In
508 parallel, DDMut-PPI analysis predicted only a minimal change in binding free energy
509 between NTCP and the HBV preS1 domain upon introduction of the AAAA mutation,
510 further supporting the conclusion that this motif does not directly contribute to intrinsic
511 NTCP–preS1 binding affinity. While these computational predictions cannot substitute for
512 direct biochemical binding measurements, they are consistent with prior studies identifying
513 alternative NTCP residues as the primary determinants of HBV preS1 engagement and viral
514 internalization (37-41).

515 Taken together with the comparable steady-state expression levels of NTCP WT and the

516 AAAA mutant (Fig. S2) and the markedly reduced surface localization of the AAAA
517 variant, indicative of impaired motor-dependent transport, these data support a trafficking
518 defect—rather than an intrinsic loss of receptor function—as the primary basis for the
519 reduced NTCP-mediated HBV and HDV infectivity observed for the AAAA mutant.
520 Collectively, our combined biochemical, structural, and computational analyses support a
521 model in which the NTCP leucine-rich motif is dispensable for direct viral binding but is
522 essential for KIF4-dependent NTCP recognition and surface transport, thereby indirectly
523 regulating HBV and HDV entry.

524 Integrin β1 (ITGB1/CD29) is a transmembrane protein that forms functional
525 heterodimers with multiple α-integrin subunits, including ITGA2 and ITGA3, thereby
526 generating receptors that are essential for cellular homeostasis. Through binding to
527 extracellular matrix (ECM) components such as laminin, collagen, and fibronectin, ITGB1-
528 containing integrins physically link the ECM to the intracellular cytoskeleton and regulate
529 key cellular processes, including adhesion, proliferation, migration, and gene expression
530 (42, 43). Beyond these physiological functions, ITGB1 heterodimers also serve as entry
531 factors for a variety of viruses (43-47) and contribute to tumor invasion and metastasis by
532 enabling cancer cells to adhere to the basement membrane of target tissues (48).
533 Collectively, these properties position ITGB1 as an attractive antiviral and anticancer target.
534 In this context, elucidating the molecular mechanisms determining KIF4-dependent ITGB1
535 transport may provide a strategy to selectively disrupt ITGB1 surface delivery without
536 broadly impairing other KIF4-dependent cellular functions, thereby offering a potential
537 avenue for the development of targeted antiviral and anticancer therapies.

538 Here, we provide the first mechanistic insight into how the motor protein KIF4
539 selectively recognizes specific host cargo proteins for directed trafficking to the cell
540 surface. Our findings reveal that surface protein delivery is a highly organized and tightly
541 regulated process, in which defined sequence determinants enable selective engagement
542 with distinct motor proteins to ensure precise spatial localization. This work advances our
543 understanding of motor-driven secretory pathways and highlights cargo-specific
544 recognition as a key principle governing intracellular transport to the plasma membrane.
545

546 **Acknowledgement**

547 We gratefully acknowledge Dr. John Taylor at the Fox Chase Cancer Center, the USA for
548 providing pSVLD3 plasmid, Toru Hirota at JFCR, Japan for providing Myc-tagged KIF4;
549 Dr. Hiroyuki Miyoshi at RIKEN, Japan, for providing HA-tagged NTCP. This study was
550 supported by Grants in aid for Scientific Research C, 23K06575 and the Research Program
551 on Hepatitis B from AMED (grants number: 26fk0310532s0102; and 26fk0310528s0102)
552 to Hussein H. Aly, and the Research Program on Hepatitis B from AMED (grant number:
553 25fk0310532h0001) to Kazuaki Chayama.
554
555
556
557
558
559

560

561

562

563

564

565 ## Figure legends

566 **FIG 1**

567 **KIF4 interacts with the C-terminal region of NTCP. (A)** Schematic representation of C-
568 terminally HA-tagged full-length NTCP (aa 1–349) and C-terminal truncation mutants
569 comprising the N-terminal 117 (aa 1–117) or 233 (aa 1–233) amino acids. **(B)** HEK293FT
570 cells were co-transfected with expression plasmids encoding Myc-tagged KIF4 and C-
571 terminally HA-tagged full-length NTCP or the indicated NTCP truncation mutants at a 1:1
572 ratio. At 72 h post-transfection, cells were lysed, and 10% of each lysate was analyzed by
573 immunoblotting to detect Myc-KIF4 (*Input; uppermost panel*), HA-NTCP (*Input; middle*
574 *panel*), and β-actin (loading control) (*Input; lowermost panel*). The remaining lysates
575 (90%) were subjected to co-immunoprecipitation using either an isotype control antibody
576 or anti-Myc antibody to pull down Myc-KIF4. Immunoprecipitates were analyzed by
577 immunoblotting for Myc-KIF4 (*IP; upper panel*) and co-immunoprecipitated HA-NTCP
578 (*IP; lower panel*). Data are representative of three independent experiments.

579

580 **FIG 2**

581 **KIF4 recognizes NTCP via a leucine-rich motif (aa 298–301) at the C-terminal end of**

582 **NTCP. (A)** Schematic representation of the NTCP truncation mutant comprising the C-
583 terminal 116 residues (aa 234–349) and full-length human ITGB1 (aa 1–798). Black boxes
584 denote the C-terminal transmembrane domains (CT-TMDs) of NTCP (aa 281–311; upper)
585 and ITGB1 (aa 729–751; lower). The shared leucine-rich motif within the CT-TMDs is
586 highlighted in yellow. **(B)** Schematic representation of C-terminally HA-tagged NTCP
587 truncation mutant (aa 234–349) either WT or carrying alanine substitutions at residues
588 L298, L299, L300, and I301. **(C)** HEK293FT cells were co-transfected with expression
589 plasmids encoding Myc-tagged KIF4 and C-terminally HA-tagged full-length NTCP or the
590 NTCP (aa 234–349) truncation mutant, either WT or carrying the indicated alanine
591 substitutions, at a 1:1 ratio. At 72 h post-transfection, cells were lysed, and 10% of each
592 lysate was analyzed by immunoblotting to detect Myc-KIF4 (*Input; uppermost panel*), HA-
593 NTCP (*Input; middle panel*), and β-actin (loading control) (*Input; lowermost panel*). The
594 remaining lysates (90%) were subjected to co-immunoprecipitation using either an isotype
595 control antibody or anti-Myc antibody to pull down Myc-KIF4. Immunoprecipitates were
596 analyzed by immunoblotting for Myc-KIF4 (*IP; upper panel*) and co-immunoprecipitated
597 HA-NTCP (*IP; lower panel*). Data are representative of three independent experiments.
598
599 **FIG 3**
600 **KIF4 selectively recognizes ITGB1 via a leucine-rich motif (amino acids 747–750) at**
601 **the C-terminal end of ITGB1. (A)** Schematic representation of C-terminally HA-tagged
602 full-length human ITGB1 (aa 1–798) either WT or harboring alanine substitutions at
603 residues L747, L748, L749, and I750. **(B)** HEK293FT cells were co-transfected with

604 expression plasmids encoding Myc-tagged KIF4 and C-terminally HA-tagged full-length
605 ITGB1 either WT or carrying the indicated alanine substitutions, at a 1:1 ratio. At 72 h
606 post-transfection, cells were lysed, and 10% of each lysate was analyzed by
607 immunoblotting to detect Myc-KIF4 (*Input; uppermost panel*), HA-ITGB1 (*Input; middle*
608 *panel*), and β-actin (loading control) (*Input; lowermost panel*). The remaining lysates
609 (90%) were subjected to co-immunoprecipitation using either an isotype control antibody
610 or anti-Myc antibody to pull down Myc-KIF4. Immunoprecipitates were analyzed by
611 immunoblotting for Myc-KIF4 (*IP; upper panel*) and co-immunoprecipitated HA-ITGB1
612 (*IP; lower panel*). Data are representative of three independent experiments.
613
614 **FIG 4**
615 **The NTCP C-terminal leucine-rich motif (aa 298–301) is required for KIF4-dependent**
616 **surface trafficking and HBV/HDV entry. (A)** HepG2 cells were transfected with
617 plasmids expressing C-terminally HA-tagged full-length NTCP WT ($NTCP^{WT}$) or carrying
618 the L298A, L299A, L300A, I301A substitutions ($NTCP^{AAAA}$). At 72 h post-transfection,
619 the cells were surface-biotinylated or PBS-treated at 4°C for 30 min. prior to cell lysis. Ten
620 percent of each lysate was analyzed by immunoblotting to detect total NTCP (*Input; upper*
621 *panel*), and β-actin (loading control) (*Input; lower panel*). The remaining lysates were
622 incubated with streptavidin (SA) beads to isolate biotinylated surface proteins. Eluted
623 fractions were analyzed by immunoblotting to detect surface NTCP (*Surface; upper panel*)
624 and CDH-1 (loading control for surface fraction) (*Surface; lower panel*). **(B)** HepG2 cells
625 ectopically expressing $NTCP^{WT}$ or $NTCP^{AAAA}$ were incubated with 40 nM C-terminal

626 TAMRA-labeled and N-terminally myristoylated preS1 peptide (preS1 probe) for 30 min at
627 37°C; Red and blue signals indicate the preS1 probe binding and nuclei, respectively. **(C)**
628 Quantification of relative fluorescence intensity from panel B. **(D)** Schematic diagram
629 depicting the scheme for plasmid transfection and subsequent HBV infection in HepG2;
630 HepG2 cells were transfected with Mock, $NTCP^{WT}$, or $NTCP^{AAAA}$ plasmids for 72 h,
631 followed by HBV inoculation (10,000 GEq/cell) in the presence of 4% PEG8000 for 16 h.
632 After washing out free viral particles, the cells were cultured for an additional 7 days,
633 followed by detection of different HBV markers. **(E)** Intracellular HBV pgRNA levels were
634 quantified by RT-qPCR and presented as fold changes, relative to $NTCP^{WT}$ transfected
635 cells. **(F)** secreted HBeAg levels in the culture supernatant was measured by ELISA and
636 presented as (A/CO) values. **(G)** HepG2 expressing $NTCP^{WT}$ or $NTCP^{AAAA}$ were
637 inoculated with HDV (100 GEq/cell) in the presence of 5% PEG8000 for 16 h. After
638 washing and removal of the free viral particles, the cells were cultured for 6 days followed
639 by detection of intracellular HDAg by IF; Red and blue signals indicate HDAg and nuclei,
640 respectively. **(H)** Quantification of fluorescence intensity from panel G. **(I)** Cell viability
641 was also assessed by MTT assay. All assays were performed in triplicate, and data from
642 three independent experiments were included. Data are presented as mean ± SD. ***, $P <$
643 0.001; NS, not significant.
644
645 **FIG 5**
646 ***In silico* structural modeling suggests the $NTCP^{AAAA}$ substitution mutation does not**
647 **alter NTCP/preS1 binding. (A)** Panels A (a–f) show the predicted human NTCP structures

648 of the wild type and the single alanine mutants; L298A, L299A, L300A, and I301A, and
649 the quadruple mutant L298A/L299A/L300A/I301A, respectively. Panel A (g) overlays the
650 structures at the mutation sites. The colors for L298A, L299A, L300A, I301A, and
651 L298A/L299A/L300A/I301A are magenta, yellow, tint, cyan, and green, respectively. **(**B)
652 Panel B (a, b) shows the predicted human NTCP and PreS1 structures of the wild type (a)
653 and the quadruple mutant L298A/L299A/L300A/I301A (b), respectively. **(C)** Predicted
654 effects of single and quadruple alanine substitutions within the NTCP leucine-rich motif on
655 binding free energy between NTCP and the HBV preS1 domain. Individual $\Delta\Delta G^{Binding}$
656 values (kcal/mol) are shown for the single mutants (L298A, L299A, L300A, I301A), along
657 with the predicted $\Delta\Delta G^{Binding}$ (kcal/mol) for the quadruple mutant
658 (L298A/L299A/L300A/I301A).

659

660 **FIG 6**

661 **NTCP residues L298 and L299 are the minimal determinants essential for interaction**
662 **with KIF4. (A)** Schematic representation of C-terminally HA-tagged NTCP truncation
663 mutant (aa 234–349) either WT, carrying single alanine substitutions at residues L298,
664 L299, L300, or I301, or quadruple alanine substitutions (L298A/L299A/L300A/I301A). **(B)**
665 HEK293FT cells were co-transfected with expression plasmids encoding Myc-tagged KIF4
666 and C-terminally HA-tagged NTCP (aa 234–349) truncation mutant, either WT or carrying
667 the indicated alanine substitutions, at a 1:1 ratio. At 72 h post-transfection, cells were lysed,
668 and 10% of each lysate was analyzed by immunoblotting to detect HA-NTCP variants
669 (*Input; uppermost panel*), Myc-KIF4 (*Input; middle panel*), and β-actin (loading control)

670 (*Input; lowermost panel*). The remaining lysates (90%) were subjected to co-
671 immunoprecipitation using either an isotype control antibody or anti-Myc antibody to pull
672 down Myc-KIF4. Immunoprecipitates were analyzed by immunoblotting for Myc-KIF4
673 (*IP; upper panel*) and co-immunoprecipitated HA-NTCP (*IP; lower panel*). Data are
674 representative of three independent experiments.

675

676

677 **References**

678 1. Burki T. 2024. WHO's 2024 global hepatitis report. Lancet Infect Dis 24:e362-e363.
679 2. Yang S, Ye Q, Yang Y, Ma Z. 2025. Clinical impact of hepatitis delta virus coinfection on liver fibrosis
680 in hepatitis B patients: a population-based study. Virol J 22:273.
681 3. Yan H, Zhong G, Xu G, He W, Jing Z, Gao Z, Huang Y, Qi Y, Peng B, Wang H, Fu L, Song M, Chen P, Gao
682 W, Ren B, Sun Y, Cai T, Feng X, Sui J, Li W. 2012. Sodium taurocholate cotransporting polypeptide is a
683 functional receptor for human hepatitis B and D virus. Elife 1:e00049.
684 4. Gad SA, Sugiyama M, Tsuge M, Wakae K, Fukano K, Oshima M, Sureau C, Watanabe N, Kato T,
685 Murayama A, Li Y, Shoji I, Shimotohno K, Chayama K, Muramatsu M, Wakita T, Nozaki T, Aly HH.
686 2022. The kinesin KIF4 mediates HBV/HDV entry through the regulation of surface NTCP localization
687 and can be targeted by RXR agonists in vitro. PLoS Pathog 18:e1009983.
688 5. Sheng L, Hao SL, Yang WX, Sun Y. 2018. The multiple functions of kinesin-4 family motor protein
689 KIF4 and its clinical potential. Gene 678:90-99.
690 6. Martinez NW, Xue X, Berro RG, Kreitzer G, Resh MD. 2008. Kinesin KIF4 regulates intracellular
691 trafficking and stability of the human immunodeficiency virus type 1 Gag polyprotein. J Virol
692 82:9937-50.
693 7. Peretti D, Peris L, Rosso S, Quiroga S, Caceres A. 2000. Evidence for the involvement of KIF4 in the
694 anterograde transport of L1-containing vesicles. J Cell Biol 149:141-52.
695 8. Zhou J, Scherer J, Yi J, Vallee RB. 2018. Role of kinesins in directed adenovirus transport and
696 cytoplasmic exploration. PLoS Pathog 14:e1007055.
697 9. Gad SA, Abo Elwafa DA, Hussein SA, Fukano K, Kato T, Shoji I, Chayama K, Muramatsu M, Isogawa M,
698 Wakita T, Merk D, Aly HH. 2025. RXR agonist S169 inhibits HBV/HDV entry in vitro by disrupting
699 KIF4-dependent NTCP trafficking. Antiviral Res 240:106214.
700 10. Hirokawa N, Noda Y, Tanaka Y, Niwa S. 2009. Kinesin superfamily motor proteins and intracellular
701 transport. Nat Rev Mol Cell Biol 10:682-96.
702 11. Verhey KJ, Hammond JW. 2009. Traffic control: regulation of kinesin motors. Nat Rev Mol Cell Biol
703 10:765-77.
704 12. Jiang X, Ogawa T, Yonezawa K, Shimizu N, Ichinose S, Uchihashi T, Nagaike W, Moriya T, Adachi N,
705 Kawasaki M, Dohmae N, Senda T, Hirokawa N. 2023. The two-step cargo recognition mechanism of
706 heterotrimeric kinesin. EMBO Rep 24:e56864.
707 13. Sharma P, Cline HT. 2010. Visual activity regulates neural progenitor cells in developing xenopus CNS
708 through musashi1. Neuron 68:442-55.

709 14. Chui SS, Lo SM, Charmant JP, Orpen AG, Williams ID. 1999. A chemically functionalizable
710 nanoporous material. Science 283:1148-50.
711 15. Gelfond D, Borowitz D. 2013. Gastrointestinal complications of cystic fibrosis. Clin Gastroenterol
712 Hepatol 11:333-42; quiz e30-1.
713 16. Takahashi M, Wakai T, Hirota T. 2016. Condensin I-mediated mitotic chromosome assembly requires
714 association with chromokinesin KIF4A. Genes Dev 30:1931-6.
715 17. Aly HH, Suzuki J, Watashi K, Chayama K, Hoshino S, Hijikata M, Kato T, Wakita T. 2016. RNA Exosome
716 Complex Regulates Stability of the Hepatitis B Virus X-mRNA Transcript in a Non-stop-mediated
717 (NSD) RNA Quality Control Mechanism. J Biol Chem 291:15958-74.
718 18. Londino JD, Gulick DL, Lear TB, Suber TL, Weathington NM, Masa LS, Chen BB, Mallampalli RK. 2017.
719 Post-translational modification of the interferon-gamma receptor alters its stability and signaling.
720 Biochem J 474:3543-3557.
721 19. Ibrahim MK, Abdelhafez TH, Takeuchi JS, Wakae K, Sugiyama M, Tsuge M, Ito M, Watashi K, El Kassas
722 M, Kato T, Murayama A, Suzuki T, Chayama K, Shimotohno K, Muramatsu M, Aly HH, Wakita T. 2021.
723 MafF Is an Antiviral Host Factor That Suppresses Transcription from Hepatitis B Virus Core Promoter.
724 J Virol 95:e0076721.
725 20. Kuo MY, Chao M, Taylor J. 1989. Initiation of replication of the human hepatitis delta virus genome
726 from cloned DNA: role of delta antigen. J Virol 63:1945-50.
727 21. Sureau C, Guerra B, Lee H. 1994. The middle hepatitis B virus envelope protein is not necessary for
728 infectivity of hepatitis delta virus. J Virol 68:4063-6.
729 22. Ma H, Kim AS, Kafai NM, Earnest JT, Shah AP, Case JB, Basore K, Gilliland TC, Sun C, Nelson CA,
730 Thackray LB, Klimstra WB, Fremont DH, Diamond MS. 2020. LDLRAD3 is a receptor for Venezuelan
731 equine encephalitis virus. Nature 588:308-314.
732 23. Sievers F, Higgins DG. 2018. Clustal Omega for making accurate alignments of many protein
733 sequences. Protein Sci 27:135-145.
734 24. Robert X, Guillon C, Gouet P. 2025. FoldScript: a web server for the efficient analysis of AI-generated
735 3D protein models. Nucleic Acids Res 53:W277-W282.
736 25. Heintz TG, Heller JP, Zhao R, Caceres A, Eva R, Fawcett JW. 2014. Kinesin KIF4A transports integrin
737 beta1 in developing axons of cortical neurons. Mol Cell Neurosci 63:60-71.
738 26. Abramson J, Adler J, Dunger J, Evans R, Green T, Pritzel A, Ronneberger O, Willmore L, Ballard AJ,
739 Bambrick J, Bodenstein SW, Evans DA, Hung CC, O'Neill M, Reiman D, Tunyasuvunakool K, Wu Z,
740 Zemgulyte A, Arvaniti E, Beattie C, Bertolli O, Bridgland A, Cherepanov A, Congreve M, Cowen-Rivers
741 AI, Cowie A, Figurnov M, Fuchs FB, Gladman H, Jain R, Khan YA, Low CMR, Perlin K, Potapenko A,
742 Savy P, Singh S, Stecula A, Thillaisundaram A, Tong C, Yakneen S, Zhong ED, Zielinski M, Zidek A,
743 Bapst V, Kohli P, Jaderberg M, Hassabis D, Jumper JM. 2024. Accurate structure prediction of
744 biomolecular interactions with AlphaFold 3. Nature 630:493-500.
745 27. Zhou Y, Myung Y, Rodrigues CHM, Ascher DB. 2024. DDMut-PPI: predicting effects of mutations on
746 protein-protein interactions using graph-based deep learning. Nucleic Acids Res 52:W207-W214.
747 28. Zhang L, Struss A, Qin M, Dombrowski A, Li T, Viebahn S, Mehlhorn D, Grefen C. 2025. A
748 phosphoinositide-mediated switch of GET pathway receptor dimerization in Arabidopsis. Proc Natl
749 Acad Sci U S A 122:e2514354122.
750 29. Kelkar SA, Pfister KK, Crystal RG, Leopold PL. 2004. Cytoplasmic dynein mediates adenovirus binding
751 to microtubules. J Virol 78:10122-32.
752 30. Kelkar S, De BP, Gao G, Wilson JM, Crystal RG, Leopold PL. 2006. A common mechanism for
753 cytoplasmic dynein-dependent microtubule binding shared among adeno-associated virus and
754 adenovirus serotypes. J Virol 80:7781-5.
755 31. Strunze S, Engelke MF, Wang IH, Puntener D, Boucke K, Schleich S, Way M, Schoenenberger P,
756 Burckhardt CJ, Greber UF. 2011. Kinesin-1-mediated capsid disassembly and disruption of the
757 nuclear pore complex promote virus infection. Cell Host Microbe 10:210-23.

758 32. Malikov V, da Silva ES, Jovasevic V, Bennett G, de Souza Aranha Vieira DA, Schulte B, Diaz-Griffero F,
759 Walsh D, Naghavi MH. 2015. HIV-1 capsids bind and exploit the kinesin-1 adaptor FEZ1 for inward
760 movement to the nucleus. Nat Commun 6:6660.
761 33. Ravindran MS, Engelke MF, Verhey KJ, Tsai B. 2017. Exploiting the kinesin-1 molecular motor to
762 generate a virus membrane penetration site. Nat Commun 8:15496.
763 34. Goutam K, Ielasi FS, Pardon E, Steyaert J, Reyes N. 2022. Structural basis of sodium-dependent bile
764 salt uptake into the liver. Nature 606:1015-1020.
765 35. Xu Z, Zhao K, Wang J, Zhang L, Yin J, Chen N, Chen S, Zhao G, Wang M, Xin T, Zhu C, Cheng X, Xia Y.
766 2025. Screening of different species reveals cat hepatocytes support HBV infection. PLoS Pathog
767 21:e1013390.
768 36. Chen F, Wettengel JM, Gegenfurtner F, Moosmuller J, Bunse T, Jeske SD, Hagen P, Ni Y, Urban S,
769 Protzer U. 2025. Identification of NTCP animal orthologs supporting hepatitis B virus binding and
770 infection. J Virol 99:e0183324.
771 37. Yan H, Peng B, He W, Zhong G, Qi Y, Ren B, Gao Z, Jing Z, Song M, Xu G, Sui J, Li W. 2013. Molecular
772 determinants of hepatitis B and D virus entry restriction in mouse sodium taurocholate
773 cotransporting polypeptide. J Virol 87:7977-91.
774 38. Matsuzawa K, Ekimoto T, Kobayashi C, Shionoya K, Mifune J, Morita T, Takeuchi JS, Park SY, Ikeguchi
775 M, Sureau C, Kawaguchi A, Watashi K. 2026. Structural mapping of NTCP distinguishes its dual
776 functionality as a hepatitis B virus receptor and bile acid transporter. PLoS Pathog 22:e1013824.
777 39. Takeuchi JS, Fukano K, Iwamoto M, Tsukuda S, Suzuki R, Aizaki H, Muramatsu M, Wakita T, Sureau C,
778 Watashi K. 2019. A Single Adaptive Mutation in Sodium Taurocholate Cotransporting Polypeptide
779 Induced by Hepadnaviruses Determines Virus Species Specificity. J Virol 93.
780 40. Liu H, Zakrzewicz D, Nosol K, Irobalieva RN, Mukherjee S, Bang-Sorensen R, Goldmann N, Kunz S,
781 Rossi L, Kossiakoff AA, Urban S, Glebe D, Geyer J, Locher KP. 2024. Structure of antiviral drug
782 bulevirtide bound to hepatitis B and D virus receptor protein NTCP. Nat Commun 15:2476.
783 41. Zakrzewicz D, Leidolf R, Kunz S, Muller SF, Neubauer A, Leiting S, Goldmann N, Lehmann F, Glebe D,
784 Geyer J. 2022. Tyrosine 146 of the Human Na(+)/Taurocholate Cotransporting Polypeptide (NTCP) Is
785 Essential for Its Hepatitis B Virus (HBV) Receptor Function and HBV Entry into Hepatocytes. Viruses
786 14.
787 42. Liu S, Calderwood DA, Ginsberg MH. 2000. Integrin cytoplasmic domain-binding proteins. J Cell Sci
788 113 (Pt 20):3563-71.
789 43. Fu R, Jordan P, Engels Z, Weihs JA, Murle J, Chi H, Burbano de Lara S, Helm B, Klohn M, Hu J,
790 Freistaedter A, Boettler T, Binder M, Klingmuller U, Steinmann E, Lozach PY, Tubiana T, Lemon SM,
791 Dao Thi VL. 2025. Integrin beta 1 facilitates non-enveloped hepatitis E virus cell entry through the
792 recycling endosome. Nat Commun 16:5403.
793 44. Shuai L, Wang J, Zhao D, Wen Z, Ge J, He X, Wang X, Bu Z. 2020. Integrin beta1 Promotes Peripheral
794 Entry by Rabies Virus. J Virol 94.
795 45. Izmailyan R, Hsao JC, Chung CS, Chen CH, Hsu PW, Liao CL, Chang W. 2012. Integrin beta1 mediates
796 vaccinia virus entry through activation of PI3K/Akt signaling. J Virol 86:6677-87.
797 46. Kaminsky PM, Keiser NW, Yan Z, Lei-Butters DC, Engelhardt JF. 2012. Directing integrin-linked
798 endocytosis of recombinant AAV enhances productive FAK-dependent transduction. Mol Ther
799 20:972-83.
800 47. Rivera-Serrano EE, Gonzalez-Lopez O, Das A, Lemon SM. 2019. Cellular entry and uncoating of naked
801 and quasi-enveloped human hepatoviruses. Elife 8.
802 48. Hood JD, Cheresh DA. 2002. Role of integrins in cell invasion and migration. Nat Rev Cancer 2:91-
803 100.
804
805
806

807 ## Supplementary figure legends

808 **FIG S1**

809 **Sequence alignment of the NTCP C-terminal region with human ITGB1.** Alignment of
810 the C-terminal 116 amino acids of NTCP (aa 234–349) with human ITGB1. Conserved
811 residues and regions of sequence similarity are marked or highlighted.

812

813 **FIG S2**

814 **Protein expression of NTCP and ITGB1 (WT *vs* quadruple alanine mutant) in**
815 **HEK293 FT cells.** HEK293FT cells were transfected with mock plasmid or plasmids
816 expressing C-terminally HA-tagged full-length NTCP WT, NTCP carrying
817 L298A/L299A/L300A/I301A substitutions, C-terminally HA-tagged full-length ITGB1
818 WT, or ITGB1 harboring L747A/L748A/L749A/I750A substitutions. At 72 h post-
819 transfection, cells were lysed and analyzed by immunoblotting to detect NTCP or ITGB1
820 (*upper panel*) and β-actin (*lower panel*; loading control). Data are representative of three
821 independent experiments. Data are representative of three independent experiments.

822

823 **FIG S3**

824 **Sequence alignment of NTCP residues 294–305 within the C-terminal transmembrane**
825 **region across HBV-susceptible species.** The C-terminal transmembrane segment (aa 294–
826 305) of NTCP orthologs from human (*Homo sapiens*), cat (*Felis catus*), rabbit (*Oryctolagus*
827 *cuniculus*), ferret (*Mustela putorius furo*), woodchuck (*Marmota marmota*), big brown bat
828 (*Eptesicus fuscus*), aardvark (*Orycteropus afer afer*), horse (*Equus caballus*), chinese tree

829 shrew (*Tupaia chinensis*), whale (*Balaenoptera acutorostrata scammony*) was shown.
830 Residues corresponding to the putative leucine-rich motif identified in human NTCP are
831 highlighted in purple.
832

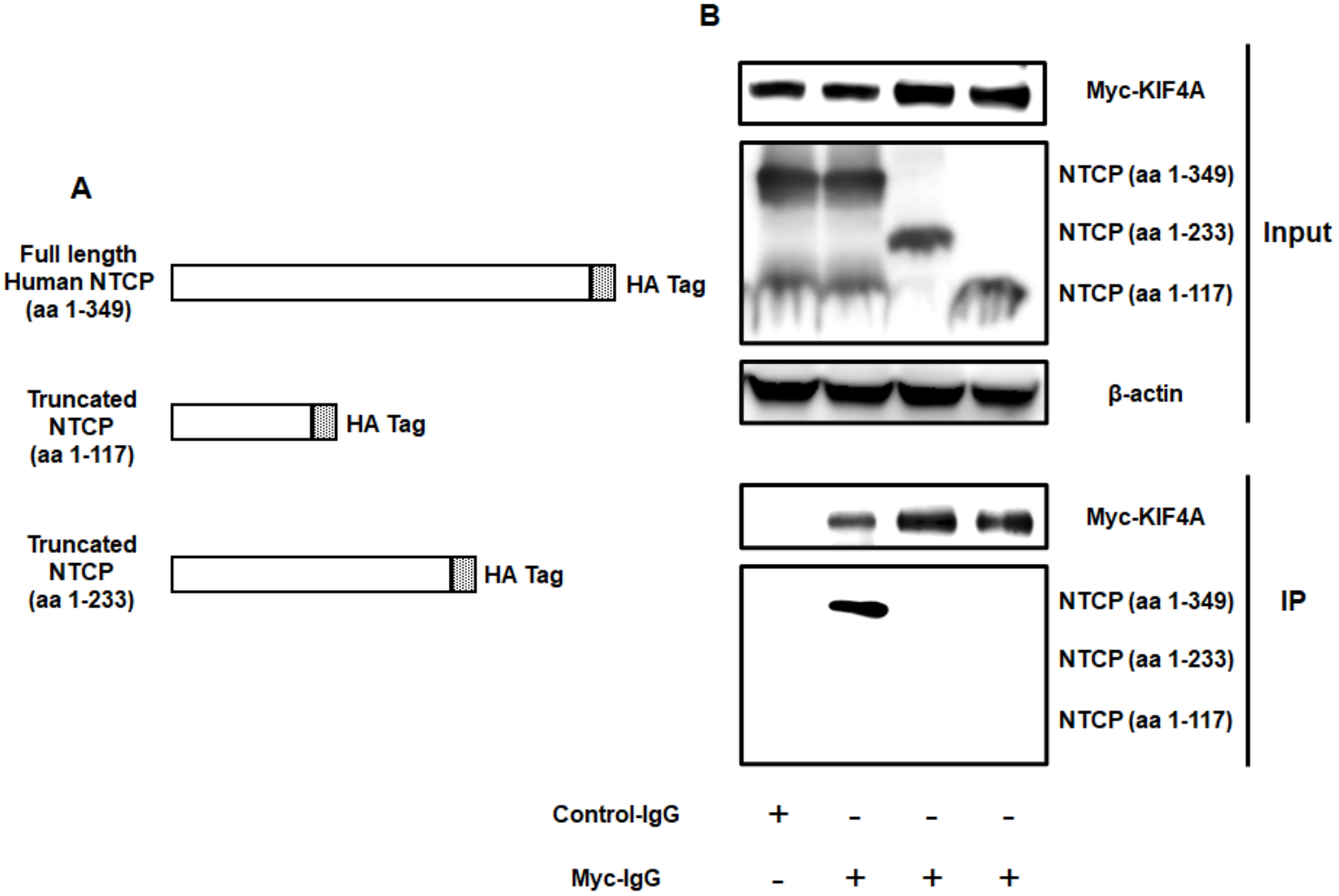
A
Full length
Human NTCP
(aa 1-349)
HA Tag
Truncated
NTCP
(aa 1-117)
HA Tag
Truncated
NTCP
(aa 1-233)
HA Tag
B
Myc-KIF4A
NTCP (aa 1-349)
NTCP (aa 1-233)
NTCP (aa 1-117)
β-actin
Input
Myc-KIF4A
NTCP (aa 1-349)
NTCP (aa 1-233)
NTCP (aa 1-117)
IP
Control-IgG + - - -
Myc-IgG - + + +

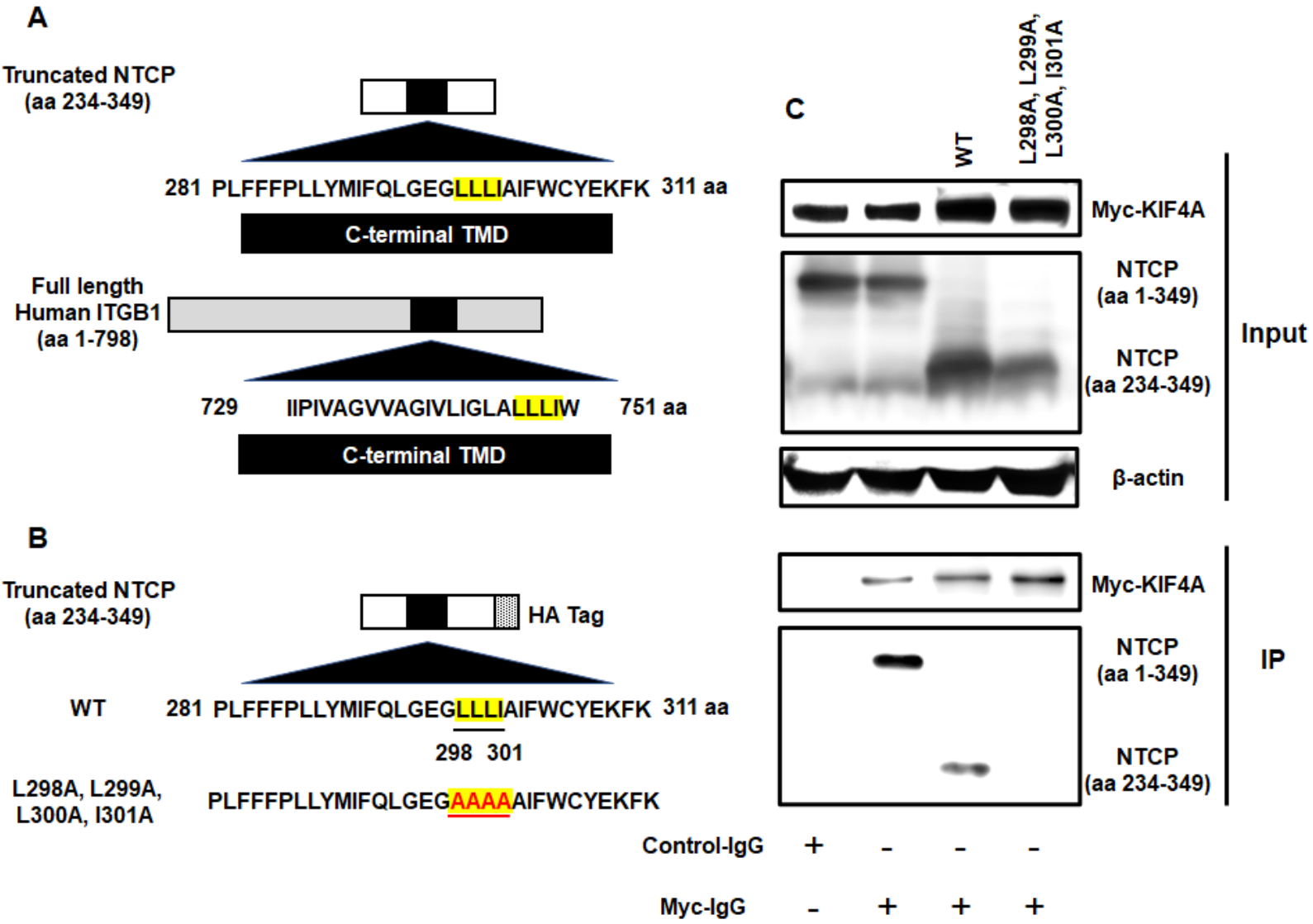
A
Truncated NTCP
(aa 234-349)
281 PLFFFPLLYMIFQLGEGLLLIAIFWCYEKFK 311 aa
C-terminal TMD
Full length
Human ITGB1
(aa 1-798)
729 IIPIVAGVVAGIVLIGLALLLIW 751 aa
C-terminal TMD
B
Truncated NTCP
(aa 234-349)
HA Tag
WT 281 PLFFFPLLYMIFQLGEGLLLIAIFWCYEKFK 311 aa
298 301
L298A, L299A,
L300A, I301A
PLFFFPLLYMIFQLGEGAAAAAIFWCYEKFK
C
WT
L298A, L299A,
L300A, I301A
Myc-KIF4A
NTCP
(aa 1-349)
NTCP
(aa 234-349)
β-actin
Input
Myc-KIF4A
NTCP
(aa 1-349)
NTCP
(aa 234-349)
IP
Control-IgG + - - -
Myc-IgG - + + +

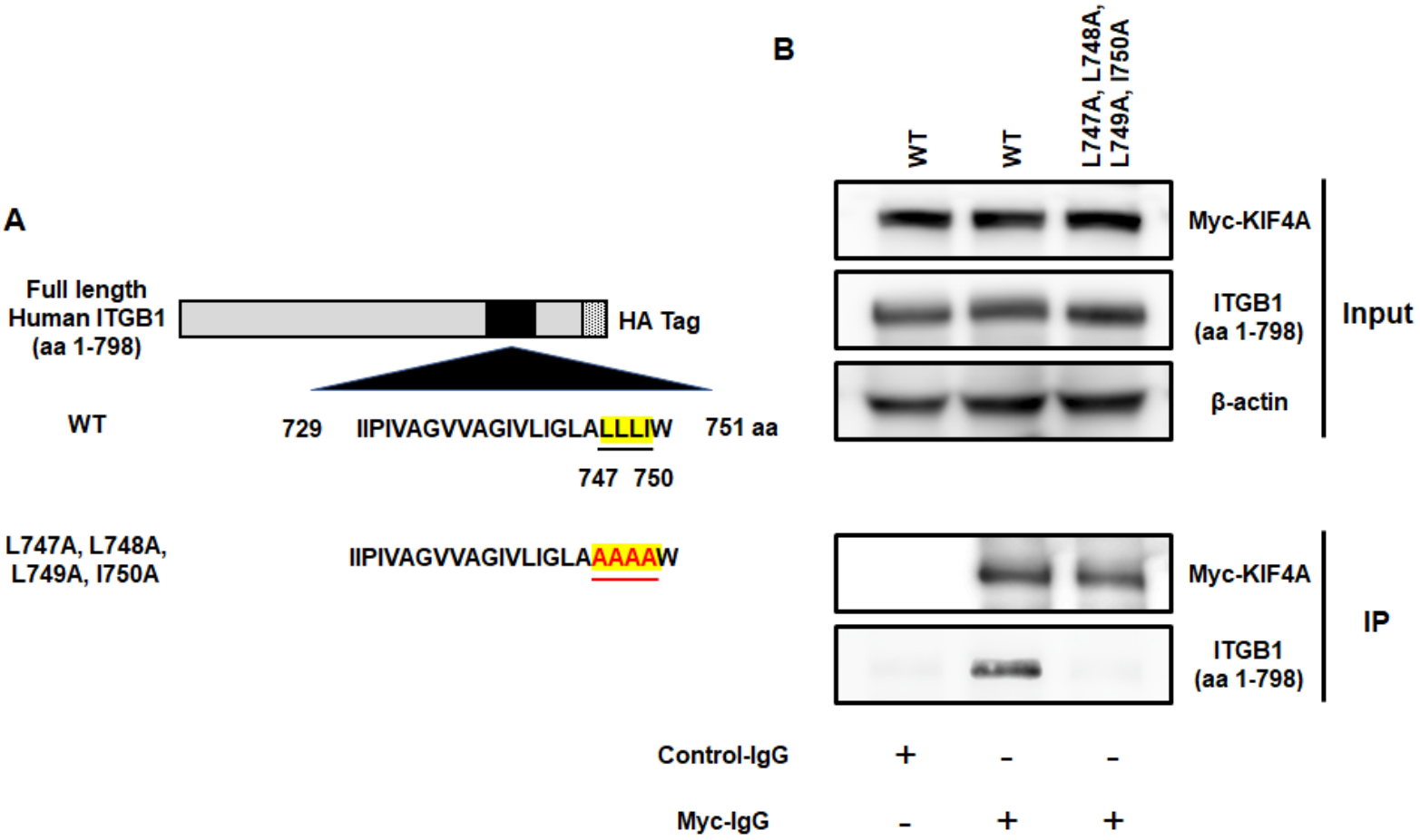
A
Full length
Human ITGB1
(aa 1-798)
HA Tag
WT
729
IIPIVAGVVAGIVLIGLALLLIW
751 aa
747
750
L747A, L748A,
L749A, I750A
IIPIVAGVVAGIVLIGLAAAAAW
B
WT
WT
L747A, L748A,
L749A, I750A
Myc-KIF4A
ITGB1
(aa 1-798)
β-actin
Input
Myc-KIF4A
ITGB1
(aa 1-798)
IP
Control-IgG
+
-
-
Myc-IgG
-
+
+

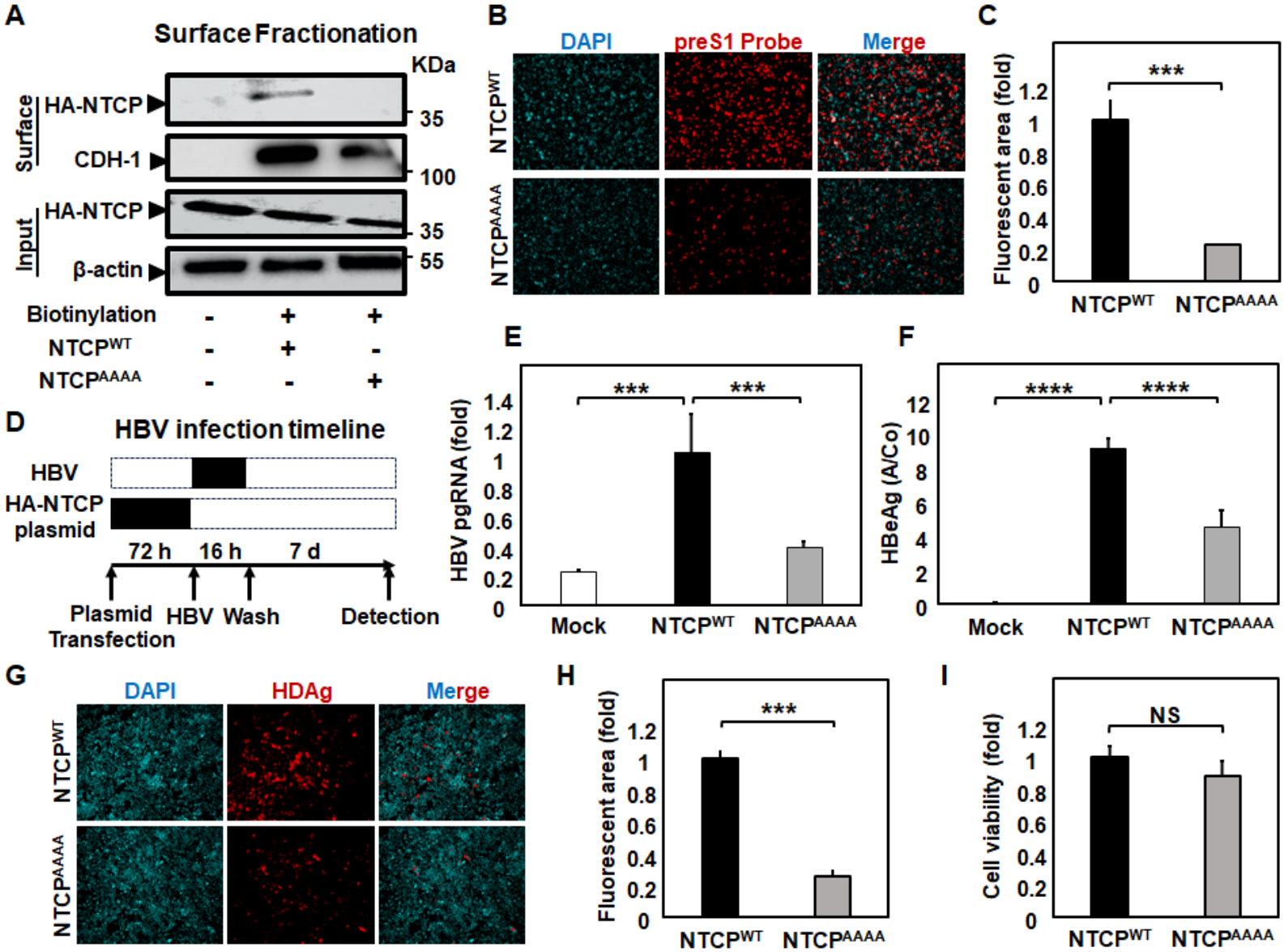
A
Surface Fractionation
KDa
Surface
HA-NTCP
CDH-1
Input
HA-NTCP
β-actin
35
100
35
55
Biotinylation - + +
NTCPWT - + -
NTCPAAAA - - +
B
DAPI
preS1 Probe
Merge
NTCPWT
NTCPAAAA
C
Fluorescent area (fold)
***
NTCPWT
NTCPAAAA
D
HBV infection timeline
HBV
HA-NTCP plasmid
72 h
16 h
7 d
Plasmid Transfection
HBV
Wash
Detection
E
HBV pgRNA (fold)
***
***
Mock
NTCPWT
NTCPAAAA
F
HBeAg (A/Co)
****
****
Mock
NTCPWT
NTCPAAAA
G
DAPI
HDAg
Merge
NTCPWT
NTCPAAAA
H
Fluorescent area (fold)
***
NTCPWT
NTCPAAAA
I
Cell viability (fold)
NS
NTCPWT
NTCPAAAA

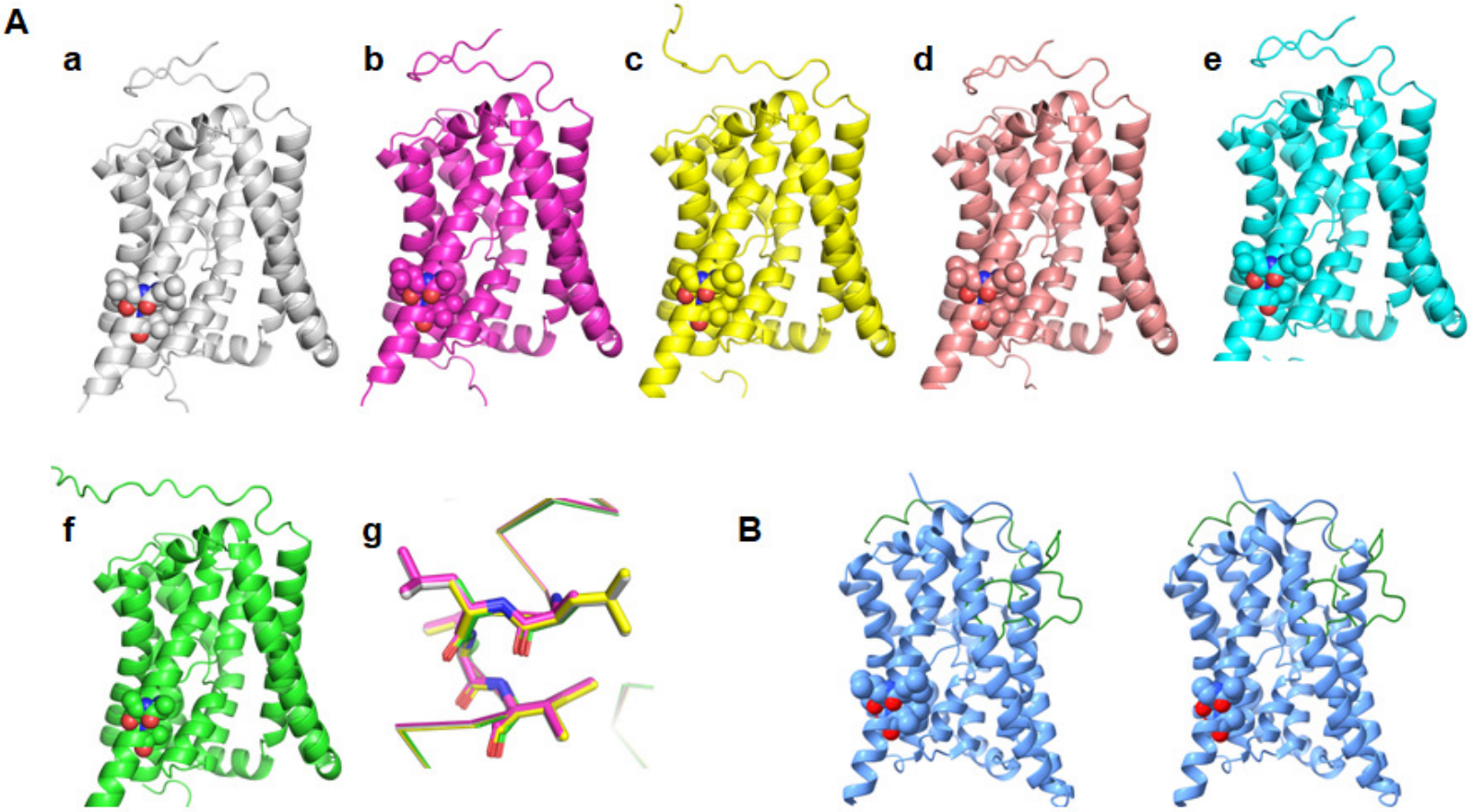

C

NTCP (PDB ID:8RQF) mutation	Average distance (Å)	Individual $\Delta\Delta G^{Binding}$ kcal/mol	Predicted $\Delta\Delta G^{Binding}$ kcal/mol
A L298A; A L299A; A L300A; A I301A	4.56	{'A L298A': -0.24567555, ' A L299A': -0.29362273, ' A L300A': -0.26692277, ' A I301A': -0.30670142}	-1.11

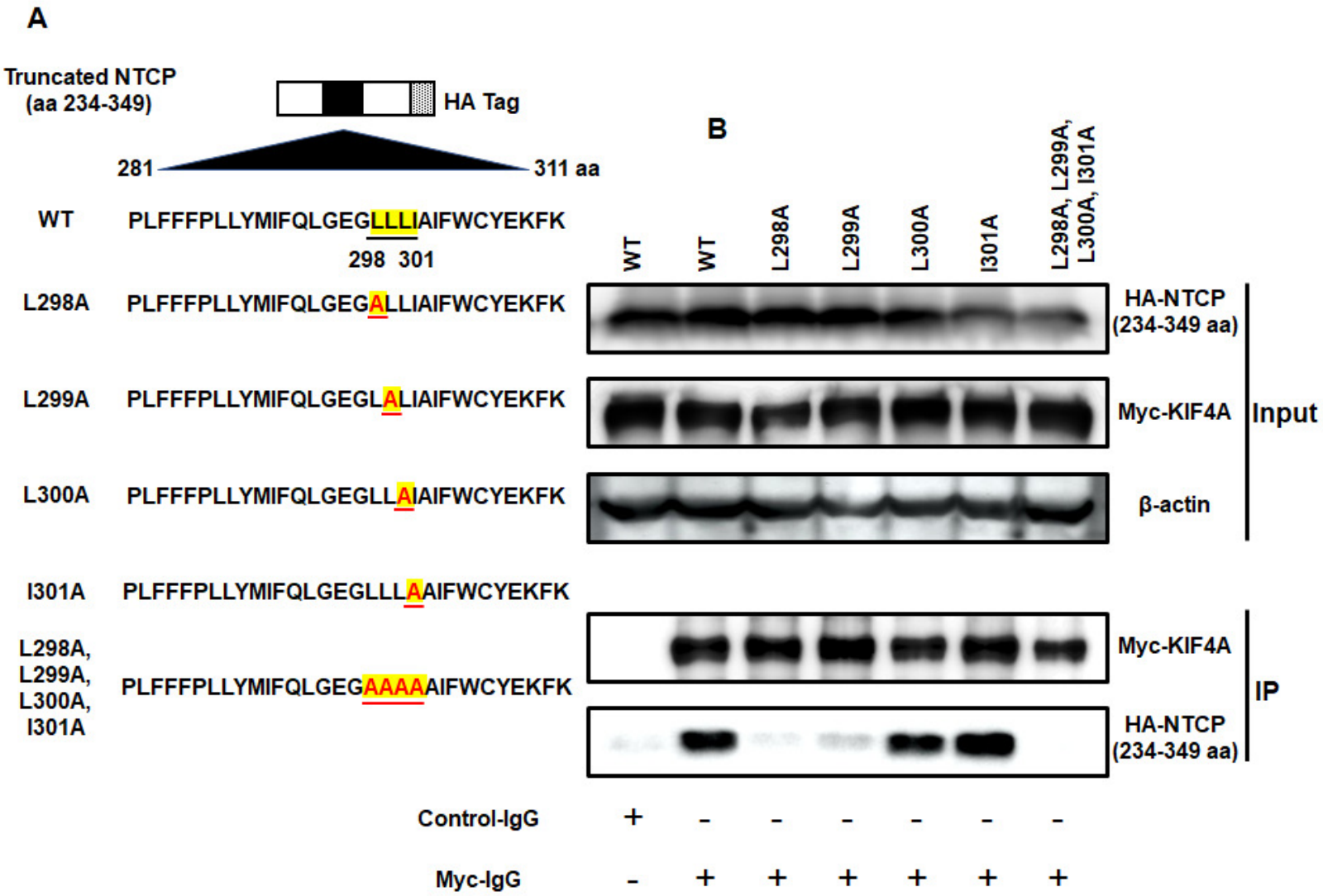
A
Truncated NTCP
(aa 234-349)
HA Tag
281
311 aa
WT PLFFFPLLYMIFQLGEGLLLIAIFWCYEKFK
298 301
L298A PLFFFPLLYMIFQLGEGALLIAIFWCYEKFK
L299A PLFFFPLLYMIFQLGEGLALIAIFWCYEKFK
L300A PLFFFPLLYMIFQLGEGLLAIAIFWCYEKFK
I301A PLFFFPLLYMIFQLGEGLLLAAIFWCYEKFK
L298A, L299A, L300A, I301A PLFFFPLLYMIFQLGEGAAAAAIFWCYEKFK
B
WT
WT
L298A
L299A
L300A
I301A
L298A, L299A, L300A, I301A
HA-NTCP (234-349 aa)
Myc-KIF4A
β-actin
Input
Myc-KIF4A
HA-NTCP (234-349 aa)
IP
Control-IgG + - - - - - -
Myc-IgG - + + + + + +